A plasmonically-enhanced route to faster and more energy-efficient phase-change integrated photonic memory and computing devices

E. Gemo,[1] J. Faneca,[1] S. G.-C. Carrillo[1], A. Baldycheva,[1] W. H. P. Pernice,[2] H. Bhaskaran[3] and C. D. Wright[1,a)]

[1]*Department of Engineering, University of Exeter, Exeter EX4 4QF, UK*

[2]*Department of Physics, University of Münster, Heisenbergstr. 11, 48149 Münster, Germany*

[3]*Department of Materials, University of Oxford, Parks Road, OX1 3PH, Oxford, UK*

Over the past 30 years or more, chalcogenide phase-change materials and devices have generated much scientific and industrial interest, particularly as a platform for non-volatile optical and electronic storage devices. More recently, the combination of chalcogenide phase-change materials with photonic integrated circuits has begun to be enthusiastically explored and, amongst many proposals, the all-photonic phase-change memory brings the memristor-type device concept to the integrated photonic platform, opening up the route to new forms of unconventional (e.g. in-memory and neuromorphic) yet practicable optical computing. For any memory or computing device, fast switching speed and low switching energy are most attractive attributes, and approaches by which speed and energy efficiency can be improved are always desirable. For phase-change material based devices, speed and energy consumption are both enhanced the smaller the volume of phase-change material that is required to be switched between its amorphous and crystalline phases. However, in conventional integrated photonic systems, the optical readout of nanometric-sized volumes of phase-change material is problematic. Plasmonics offers a way to bypass such limitations: plasmonic resonant structures are inherently capable of harnessing and focussing optical energy on sub-wavelength scales, far beyond the capabilities of conventional optical and photonic elements. In this work we explore various approaches to combining the three building blocks of Si-photonics, resonant plasmonic structures and phase-change materials to deliver plasmonically-enhanced integrated phase-change photonic memory and computing devices and systems, underlining the inherent technical and theoretical challenges therein.

_____

a)   Corresponding author: david.wright@exeter.ac.uk

I.   INTRODUCTION

Silicon photonics is now a relatively mature and established technology, and one that is at the very centre of the scientific community's attention[1–6]. One of the main reasons for this is the inherent energy efficiency and wider bandwidth of the optical signal transport channels, as compared to

electrical interconnects. The marked advantages of photonic circuits for signal transport mean that silicon photonics is already used extensively in data centres and for board-to-board and chip-to-chip communication, and has also seen preliminary experimental application for on-chip signal transport[7]. More recently, the combination of Si-photonics and chalcogenide phase-change materials, or PCMs, (similar to those used for example in re-writeable DVD and Blu-ray disc formats) has led to the development of novel integrated optical memory and computing devices[8–13]. Here, the low-loss, high-bandwidth and innate parallelism (e.g. via the use of wavelength division multiplexing, or WDM) of the photonic approach, in tandem with the multi-state programming capabilities of chalcogenide PCMs, portend a new generation of fast, low-power computer processors (or co-processors) that exploit in-memory and neuromorphic computing approaches[14–20].

The basic concept of the integrated phase-change optical memory device is shown in FIG. 1; a thin chalcogenide PCM layer is fabricated on the top surface of a conventional photonic integrated waveguide (see FIG. 1(a)). Specifically, the PCM here adopted is the archetypal chalcogenide phase-change alloy $Ge_2Sb_2Te_5$ (or GST for short). Optical pulses sent down the waveguide (the 'pump' pulses in FIG. 1(a)) evanescently couple to the PCM layer and enable it to be switched between its crystalline and amorphous states, or to one of many intermediate levels of crystallinity lying between these states. Since the refractive index of PCMs is highly phase-state dependent, as shown in FIG. 1(b), the programmed phase-state of the PCM layer in turn controls (or programs) the optical transmission of the waveguide, and it is this transmission modulation that is used in the readout process (indicated by the 'probe' pulse in FIG. 1(a)) to determine the 'information' stored in the PCM cell.

As of today, up to 35 levels (>5 bit) can be reliably read, written and erased on a single PCM cell[11], and a demonstrative 512 bit memory device has also been successfully fabricated and tested[12]. Additionally, multi-state PCM cells of the type shown in FIG 1 have been used to provide arithmetic functionality[15,18], have been incorporated into novel photonic crossbar arrays to deliver ultra-fast matrix-vector multipliers[17], have been used to realise synaptic and neuronal 'mimics'[10] and even small-scale neuromorphic processors[14].

The 'conventional' phase-change photonic unit cell of FIG. 1, however, typically requires switching energies of a few hundred pJ, and switching times in the tens to hundreds of nanoseconds[8,9,11]. Approaches that can reduce switching energy requirements, and increase switching speeds, will obviously be of much benefit. Since the PCM switching process is bound to unavoidable fundamental physical limitations, namely the heating of the PCM unit cell, improvements in switching speed and energy are most likely to be achieved via two scenarios: a reduction of the unit-cell volume, or a magnification of the light-matter interaction. Plasmonics can provide us with access to both these scenarios. Indeed, plasmonics offers additional light

manipulation tools, otherwise inaccessible with conventional photonics. The collective oscillation of conduction electrons in a suitably shaped metallic nanoparticle (the so-called *localized surface plasmon*, LSP) can couple with the impinging radiation, which in turn squeezes light into much reduced volumes, and greatly magnifies the local electric field, usually leading to a much reduced (non-diffraction limited) device footprint. In this work we aim to underline the as yet untapped potential for the realisation of fast, energy-efficient photonic memory and computing devices arising from the union of the energy-efficient silicon photonics platform, the sub-wavelength light-squeezing and field-enhancing capability of plasmonic resonant structures, and the intrinsic tuneability functionality brought by PCMs.
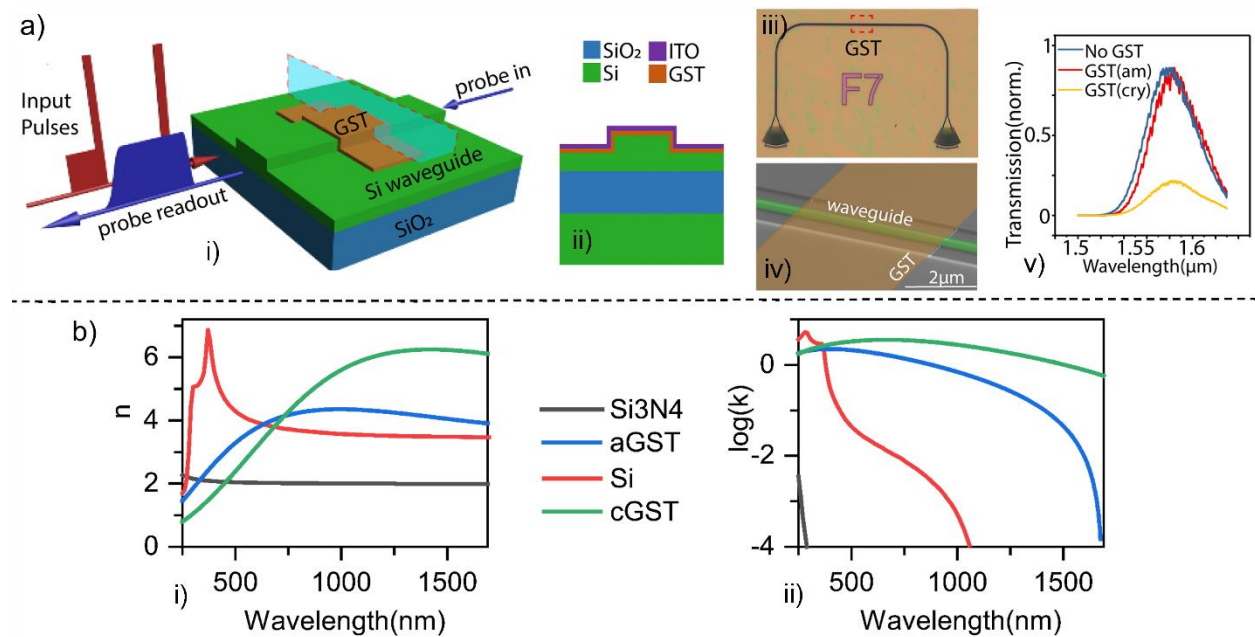

FIG. 1. Photonic Phase-Change Memory device schematics and operative principles (reprinted with permission from Ref.[16]). a) Device geometry and experimental data. (i) Device architecture and schematic of operating principle. ii) Device cross-section as represented in (i). (iii) Optical image of a test device. (iv) SEM image of the device represented in (iii). (v) Transmission data for the device in (iii) as a function of the wavelength. b) Refractive index (i) and extinction coefficient (ii) of the device materials.

II. A SHORT OVERVIEW OF PLASMONICS-ENHANCED PHOTONICS

The general light manipulation properties offered by metallic resonant nanoantennas have been widely reported (see e.g. Refs.[21–28]). The application potential of plasmonically-enhanced conventional silicon photonics devices (i.e. those not incorporating PCMs) is also quite well explored, with plasmonically-enhanced Si-photonics having already been demonstrated for

3

sensing[29–32], optical nanofocusing[33], lasing[34], emitters[35], optical mode control[36–38] and coupling[39], scattering control[40,41], photodetectors[42], and more. Also the use of hybrid plasmonic waveguides, either SPP (surface plasmon-polariton) or MIM (metal-insulator-metal) types, has been successfully demonstrated for applications such as Mach-Zehnder modulators[43–46], detectors[47], signal amplifiers[48], modulators[49], and switches[50].

In many of the cases discussed above, the properties/performances of the various plasmonically-enhanced waveguide devices were locked-in at the design stage, though some hybrid plasmonic waveguide concepts do offer tuneability[43–45,47–50] in their response. Tuning of the response of metallic nanostructures can be roughly classified in two general cases: methods directly modifying the metal dielectric function (e.g. carrier injection), and methods inducing a variation of the dielectric function of the surrounding environment (e.g. carrier injection and carrier generation, thermo-optic effects, liquid crystals, chemical adsorption, photochromic molecules, MEMS-NEMS, matter displacement, and, the focus of this work, PCM approaches). The use of PCMs to engender tuneability in plasmonic devices is particularly attractive, since PCMs have the appealing characteristics of both non-volatility and a remarkably large variation of optical properties between phases (amorphous and crystalline states). For example, as seen in FIG. 1(b), the archetypal PCM alloy GST exhibits, in the near IR, differences in the real and imaginary parts of the refractive index of around $\Delta n_{max} > 2$ and $\Delta \kappa_{max} > 1$. Indeed, the combination of PCMs with plasmonic nanostructures to provide active, dynamically tuneable (or reconfigurable) optical metasurfaces for the control of free-space light propagation is now quite a well-explored topic (see e.g. Ref.[51]), but the exploitation of PCMs to tune waveguide-mounted plasmonic devices is, at present, rather underexplored. We therefore discuss such a topic in the following sections.

III. PHASE-CHANGE ENABLED TUNEABILITY OF ON-CHIP PLASMONIC DEVICES

An early proposal which saw the combination of phase-change materials with plasmonics in an integrated silicon photonics type platform is found in Rudé et al.[49] (see FIG. 2(a)). The authors demonstrated the transmission tunability of a hybrid Au/SiO₂ plasmonic waveguide, by varying the crystal fraction of an 80 nm thick GST layer fabricated on top of the waveguide's surface. Switching of the PCM layer was here attained through an off-plane laser pulse, although electrical switching was also suggested as a possibility by the authors. The device shows a superior optical contrast when compared to alternative techniques for SP waveguide attenuation tunability, and whilst the authors underline how the switching energy is rather high (a 6.9 nJ figure is reported), the PCM non-volatility (and thus, the passive retention of the waveguide attenuation) is indeed an alluring and energy-efficient characteristic, compared to volatile technologies.

Another, and quite recent, proposal for combining PCMs with plasmonically-enhanced photonic integrated circuit (PIC) devices include that reported by Zhang et al.[52] and shown in FIG. 2(b). This reprises Rudé's concept for modulating SPP propagation, although this time in a MIM waveguide, with a GST region contiguous to (or interjecting) the dielectric core of the waveguide. The authors use this idea to configure both integrated switches and modulators. The study is purely numerical, and it does not pursue practical switching solutions, although the authors also propose the use of an external laser source. Additionally, the MIM waveguide inherits the high insertion loss (IL) previously seen in Rudé et al. Yet, the concept shows how a drastic reduction of the modulator footprint can be achieved, while maintaining a high optical contrast (here of up to ~70%) by use of a GST inclusion measuring only 50 nm × 200 nm in size. This result highlights the potential for very small volumes of PCM to yield excellent control of waveguide propagation, when combined with appropriate plasmonic structures.
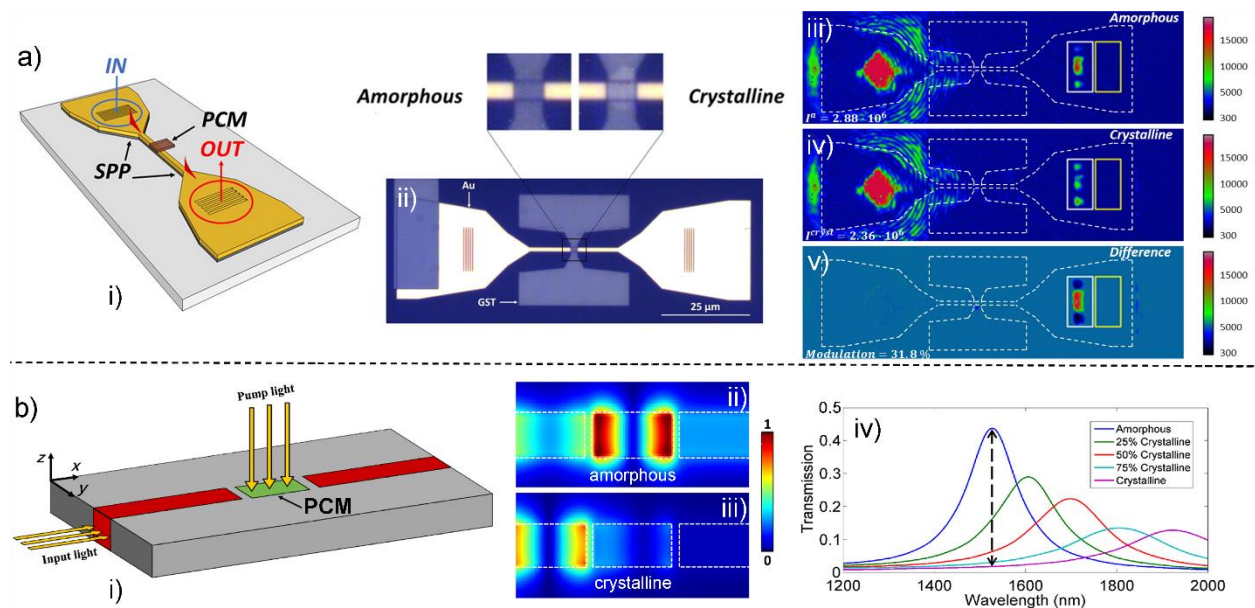

FIG. 2. GST-enabled SP propagation tuneable devices. a) Au/PCM hybrid waveguide (Reprinted with permission from Rudé et al.[49]). (i) Device schematic representation. (ii) Optical microscope image of the fabricated device; inserts highlight the device with the GST in its amorphous and crystal phases. (iii-iv) Intensity images of the scattered and transmitted light at λ = 1550 nm for the GST in its amorphous and crystal phases respectively. (v) Difference of the collected signals reported in (iii) and (iv), demonstrating the optical contrast capability. Colour bar in arbitrary units. b) Tuneable propagation on MIM waveguide concept (Reprinted with permission from Zhang et al.[52]). (i) Device schematic representation. (ii) Calculated transmission as a function of the GST inclusion crystal fraction. (iii-iv) Simulated electric field (normalised; colour bar on the right) in the amorphous and crystal phases respectively.

The work highlighted in FIG. 2 is concerned with modulator solutions that tune and control the propagation of SPPs. In Singh et al.[53], the combination of plasmonics and PCM technology with more conventional silicon photonics platforms is explored. In this (simulation-only) work, the authors propose a GST-enabled photonic modulator which enhances the absorption functionality by use of a series of optimized gold nano-rings, fabricated on top of a dielectric ridge waveguide (see FIG. 3(a)). Such a structure by itself selectively absorbs a narrow portion of the spectrum, whose bandwidth is determined by the nanorings' geometrical parameters (i.e. radius and thickness). The authors embed a nanoring array on a silicon dioxide layer, built on the top surface of a conventional rib waveguide. On top of this structure, a PCM layer is deposited and capped with an electrical contact, with the PCM switching process being carried out electrically. The absorption induced by the PCM layer, as well as the wavelength selectivity, are determined by the PCM phase. Importantly, the work of Singh et al. suggests how the use of low footprint nanostructures can have similar, if not higher, modulation performances than encountered in SPP waveguides or in MIM devices, but at a much reduced IL.

Turning to the use of the combination of PCMs and plasmonics for photonic integrated circuit (PIC) type memory and computing devices, to our knowledge, only two additional works are currently published. One, by Gemo et al.[54], seeks to improve the performance of the all-photonic phase-change memory (of the type shown in FIG. 1(a)) by exploiting the plasmonic resonance of a dimer nanoantenna fabricated on the top surface of an integrated waveguide (see FIG. 3(b)). Such a device greatly enhances the electric field magnitude in the gap between the two halves of the dimer antenna, and with a PCM layer deposited into the gap region, the device i) maximises the light-matter interaction, ii) changes its resonant properties upon variation of the phase-state (crystal fraction) of the PCM inclusion, and iii) by use of a much-reduced PCM volume, requires a fraction of the switching energy of the conventional device architecture. The numerical investigation highlights how such a device, designed in a way to allow for practicable fabrication using standard lithographic techniques, is capable of yielding an optical contrast of roughly 12.5% (maintaining an appreciably low IL of 0.38 dB), by use of a 2 pJ / 2 ns energy write (amorphization) pulse and a 15 pJ/16.5 ns erase (re-crystallization) pulse – improvements of one to two orders of magnitude as compared to the conventional device. Moreover, by use of appropriately tailored write/erase pulses, 4 memory levels were arbitrarily addressed, demonstrating the multi-level storage functionality of the plasmonically-enhanced PCM device. A later work[55] shows also the preliminary results of an experimental investigation of such devices, hinting to the confirmation of the expected behaviour.

While in the work of Gemo et al., switching of the PCM cell is achieved in the same manner as in the standard all-optical integrated phase-change memory device, i.e. by sending appropriate optical switching pulses down the waveguide, in the work of Farmakidis et al.[56] a plasmonically-enhanced
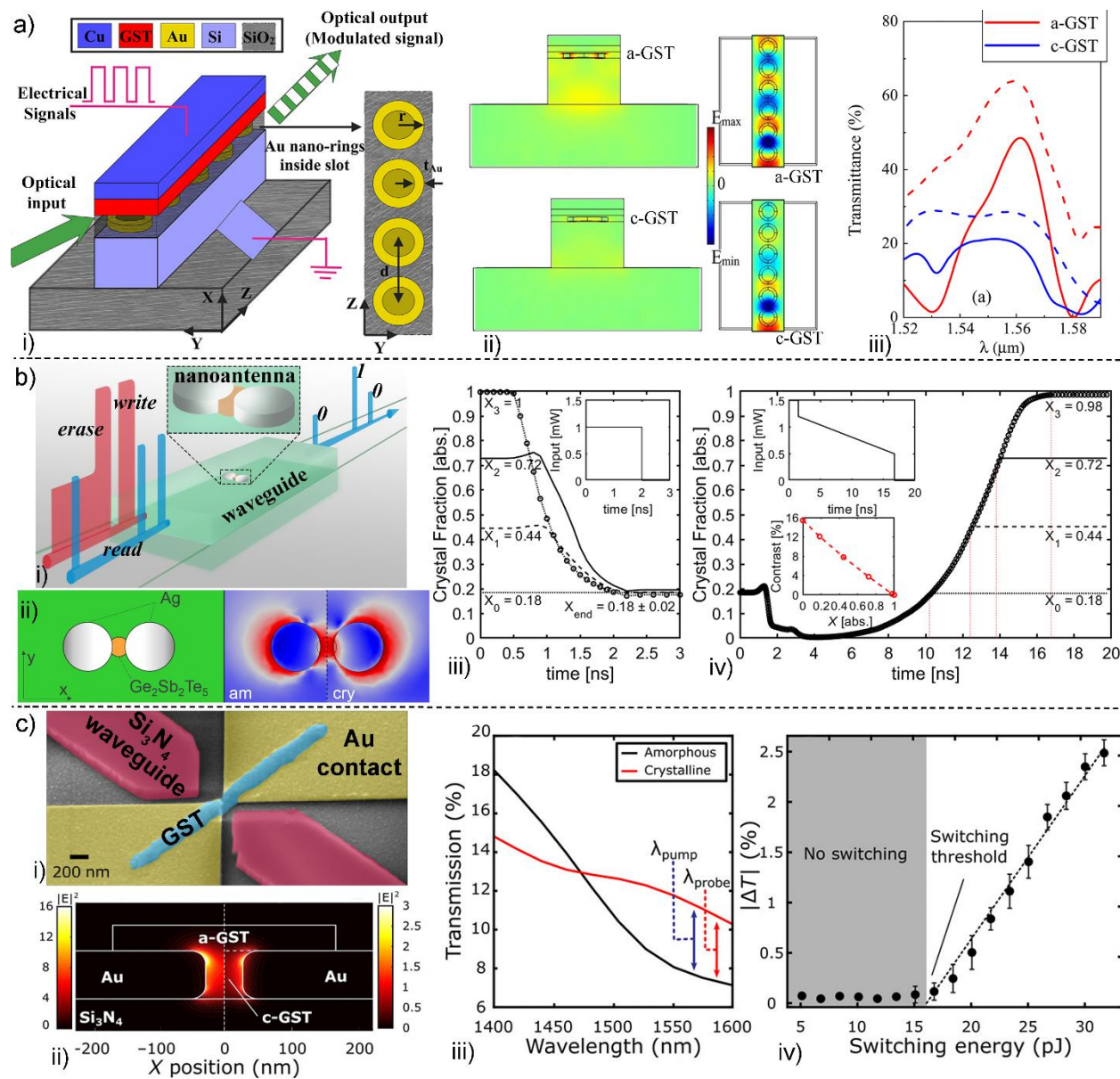
FIG. 3. Plasmonically-enhanced PCM integrated photonic devices. a) Nanoring implemented electro-optic modulator, reprinted with permission from Singh et al.[53] (i) Device schematics. (ii) Electric field distribution (normalised scale) in the amorphous (top) and crystal (bottom) phases. (iii) Wavelength- and phase-dependent transmittance. b) All-photonic phase-change memory, reprinted with permission from Gemo et al.[54]. (i) Device pictorial representation. (ii) Top view of the device (left), and log of the normalised electric field distribution across the device cut plane for amorphous and crystal GST (right). (iii-iv) Overview of the overwrite and programming operations. The insets report the pulse temporal profiles (the optical contrast is also reported as an inset in (iv)). c) Mixed-mode photonic memory, adapted with permission from Farmakidis et al.[56]. (i) False coloured SEM image of the a device. (ii) Calculated optical intensity across the device for the amorphous (left) and crystal (right) GST phases. (iii) Wavelength dependency of the optical response. (iv) Switching-energy requirement.

7

approach with dual electrical/optical switching (and dual electrical/optical reading) is proposed, and experimentally demonstrated. The concept is illustrated in FIG. 3(c). The device consists of a bow-tie like nanoantenna that interjects the dielectric waveguide, leading to the formation of a 50 nm nanogap at the waveguide centre into which a PCM layer (here again GST) is deposited. The device has a somewhat larger IL (roughly 9 dB) with respect to the all-optical solution, but a multi-level memory capability of 20 levels was successfully demonstrated, along with the aforementioned, and very attractive, capability for dual-mode (electrical/optical) operation (which makes interfacing to electronic devices considerably more straightforward). The dual-mode plasmonically-enhanced device achieved order-of-magnitude type improvements in switching energies and speeds, as compared to the conventional device architecture.

IV. PERSPECTIVES AND POSSIBLE IMPLEMENTATIONS

In section III we underlined how the use of finely tuned plasmonic nanoantennas, when combined with PCMs, gives access to a previously underexplored manipulation tool that yields useful optical contrast and low IL Si-photonic waveguide devices. A constraint on the operation speed of such devices (i.e. switching from low transmissivity to high transmissivity) remains, as it is here imposed by the phase-change dynamics (primarily the speed limitations imposed by the crystallization process), but single-nanosecond switching should almost certainly be achievable. Moreover, PCM switching is of course non-volatile, making integrated phase-change photonic devices ideal for the realization of photonic memory and (in-memory and neuromorphic) computing devices.

Previous numerical[54,56] and experimental[56] results highlight that the addition of a PCM-embedded nanogap within the plasmonic resonant structure allows one to magnify the light-matter interaction, and so modulate the device optical response in amplitude and, potentially, optical phase and scattering directivity too. The use of a nanoscale volume of PCM, which reduces the volume of material that needs to be heated during switching and so in turn reduces switching energies, would not be effective without a supporting plasmonic nanoantenna (or other resonant cavity). Indeed, the PCM volume reduction, the high volume/surface ratio, and the GST thermal boundary resistance[57], contribute to a very effective switching process, which for the all-optical plasmonically-enhanced memory device of Gemo et al.[54] sees an energy requirement of only 4.36 aJ/nm^3, quite close to the theoretical minimum of 1.9 aJ/nm^3 (calculated using values of specific heat, melting temperature and enthalpy of fusion, as reported in Ref.[54]).

One obvious drawback of following a plasmonically-enhanced device route for the provision of integrated photonic memory and computing devices is increased fabrication complexity, which in turn could lead to unacceptable variations in device-to-device properties due to fabrication

8

tolerances. This issue is examined in more detail in FIG. 4 (for the device of the type shown in FIG. 3(b)). FIG. 4(a) reports the transmission data, which determines the derived values of optical contrast (see FIG. 4(c)) and IL (FIG. 4(d)). Specifically, the introduction of the PCM in the nanogap shifts the diameter-dependent resonance feature to shorter values (smaller nanoantenna diameters), correlated with a corresponding shift (see FIG. 4(b)) of the electric field enhancement factor, EF (defined as the squared average e.m. field value in the nanogap divided by the squared peak input e.m. field value). Regardless of the phase of the PCM inclusion, it can be seen that the EF is significant, and this correlates directly with the effective optical intensity perceived by the PCM inclusion, leading to the desired increase in energy efficiency. Two optimal disc diameters for the dimer nanoantenna can be seen (in FIG. 4(c)) at around 170 nm and 250 nm, the former having a slightly higher transmission modulation (ΔT) and a smaller insertion loss (see FIG. 4(d)). However, the resonance for a 170 nm disc diameter is quite sharp, while that for 250 nm diameter is significantly broader. Thus, one may opt for the solution allowing for slightly poorer optical performance, yet increasing the fabrication tolerance. Regardless, with the steady advancement of the nanoscale fabrication techniques and establishment of improved technology nodes, it is possible to foresee how such fabrication barriers will eventually be eroded, possibly allowing one to aim designs towards the more fabrication-critical dimensioning.
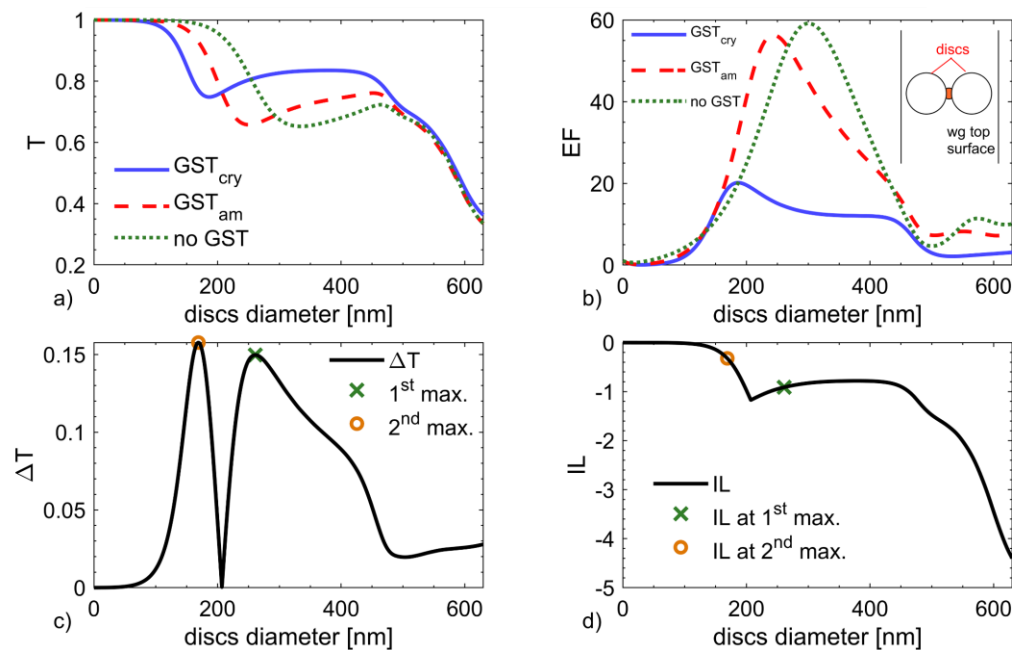

FIG. 4. Numerical analysis of the optical characteristics of the dimer-disc plasmonically-enhanced photonic PCM device, illustrated in Gemo et al.[54]. a) Transmission data, as a function of the disc diameter, for the nanoantenna-only configuration (green, dotted line) and GST-implemented configuration (blue and red lines). b) Field enhancement factor data for the three configurations, calculated at the nanogap location. c) Optical contrast $|T_{cry} - T_{am}|$ derived from the crystal and amorphous transmission data. d) Correlated minimum IL data.

We also remark that not all fabrication parameters require fine-tuning, and therefore the otherwise lengthy fabrication optimization can be limited to the most impactful parameters. As an example, the all-optical plasmonically-enhanced device shows a remarkable tolerance in terms of the nanoantenna displacement from, and rotation about, the optimal location at the centre of the top surface of the waveguide (see FIG. 5, where both dependencies can be fitted with broad sin^2 functions).

From the results presented in this section, and in the related literature[54–56] it is clear that plasmonic enhancement has the potential to drastically improve the energy and speed performance of the conventional integrated phase-change photonic memory devices. Yet, this achievement comes not only at the price of additional fabrication complexity (already discussed), but also at the reduced optical (transmission) contrast (around 20% in the best-optimized configuration). The conventional architecture can achieve much higher contrasts, simply by extending the size (along the waveguide) of the PCM unit cell, an unavailable degree of freedom for the plasmonically-enhanced cell. However, there are possible complementary strategies allowing one to not only increase the optical contrast up to (or even surpassing) that of the conventional architecture, but also to further improve device energy performance and switching speed.
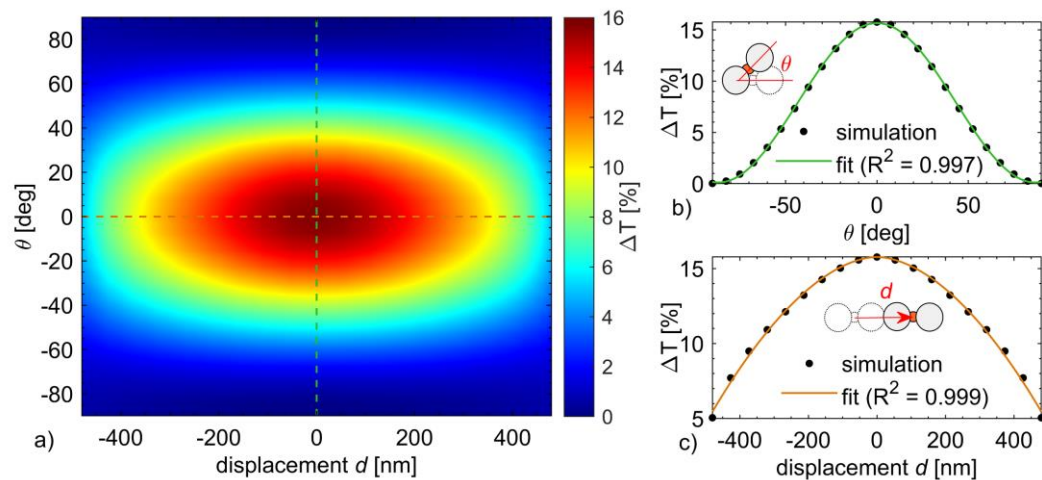

FIG. 5. Fabrication tolerance analysis of the dimer-disc nanoantenna illustrated in Gemo et al.[54], with respect to the displacement s from the waveguide centre, and from the tilting angle θ from the intended orthogonal orientation. a) Simulated ΔT as a function of displacement and tilt angle. b) Fit of the data as a function of the tilt angle, calculated at displacement $s = 0$, as: $\Delta T(\theta) = \Delta T(0) \cdot \sin^2 \theta$. c) Fit of the data as a function of the displacement s, calculated at $\theta = 0$, as: $\Delta T(s, \theta) = \Delta T(\theta) \cdot 10^{-6} \cdot (1 + \sin^2 \theta) \cdot s^{1.8}$.

One strategy consists in the adoption of multiple plasmonic structures along the waveguide. As a result of the interaction of adjacent structures, a finely tuned centre-to-centre distance (between successive nanoantennas) allows the establishment of anti-symmetric resonant modes. Such a

resonance configuration further suppresses the waveguide mode propagation and increases the e.m. field magnitude in both nanostructures, as previously demonstrated in Jin et al.[58], Therefore, two optimally located nanostructures can induce an optical contrast proportionally higher than two non-interacting nanostructures. A preliminary calculation is carried out here for the case of nanoantennas comprising two simple rectangular bars (dimer-bars) separated by a small gap (here of 40 nm), as shown in FIG. 6(a).The transmission data, FIG. 6(b), evidences a non-linear dependency of the waveguide transmission as a function of the centre-to-centre distance, with peculiar opposite behaviour for the amorphous and crystalline cases (i.e. where the crystal case shows a lowering of transmission, the amorphous case shows an increasing transmission). Both the optical contrast, ΔT, and insertion loss, IL, benefit significantly from this peculiar interaction (FIG. 6(c)), demonstrating that fact that multiple nanoantennas structures can effectively exploit characteristics offered by localized surface plasmon resonances.

Another strategy that can lead to a remarkable increase of the optical contrast is that of embedding the plasmonic nanoantenna within the body of waveguide, as shown schematically in FIG. 6(d). The effect of embedding plasmonic antennas within the body of a waveguide was previously explored in simulation by Castro-Lopez et al.[41], though for a case not including phase-change materials. For the case of dimer-bar type antennas, with PCM in the gap region and with the antenna buried at the bottom of the rib section of the waveguide, our calculations (see FIG. 6(e) and (f)) show that the maximum optical contrast doubles with respect to that obtained with the device fabricated on the top surface, with only a minor increase of the IL. This is due to the higher interaction of the plasmonic resonant mode with the natural location of the e.m. field peak within the waveguide mode. The enhancement factor here calculated increases to a value of above 100, in place of the value of 20 for the configuration with the nanoantenna on the waveguide's top surface, pointing also towards even further improvements in switching energy and speed for the embedded configuration. The embedded configuration also offers more robust protection against environmental degradation of the plasmonic and phase-change materials used in the device.

The dimer-bar type antenna configuration shown in FIG. 6 also potentially lends itself more easily to the provision of a dual-mode electrical/optical operation, as achieved in the work reported by Farmakidis et al.[56] and shown previously in FIG. 3(c), but here using a more conventional dielectric waveguide. For example, by extending the bar antennas towards the edge of the waveguide, it should be possible to make electrical connections to the bars, so that they play a dual role of both a plasmonic nanoantenna and an electrode that would allow the PCM region to be switched (or read out) electrically. One possible design for this is shown in FIG. 6(g), along with its optical performance in FIG. 6(i) and (h), from which it can be seen good optical performance can be achieved (with both optical contrast and IL greatly improved over the hybrid waveguide

11

configuration[56]), while at the same time providing electrical access for potential dual-mode operation.
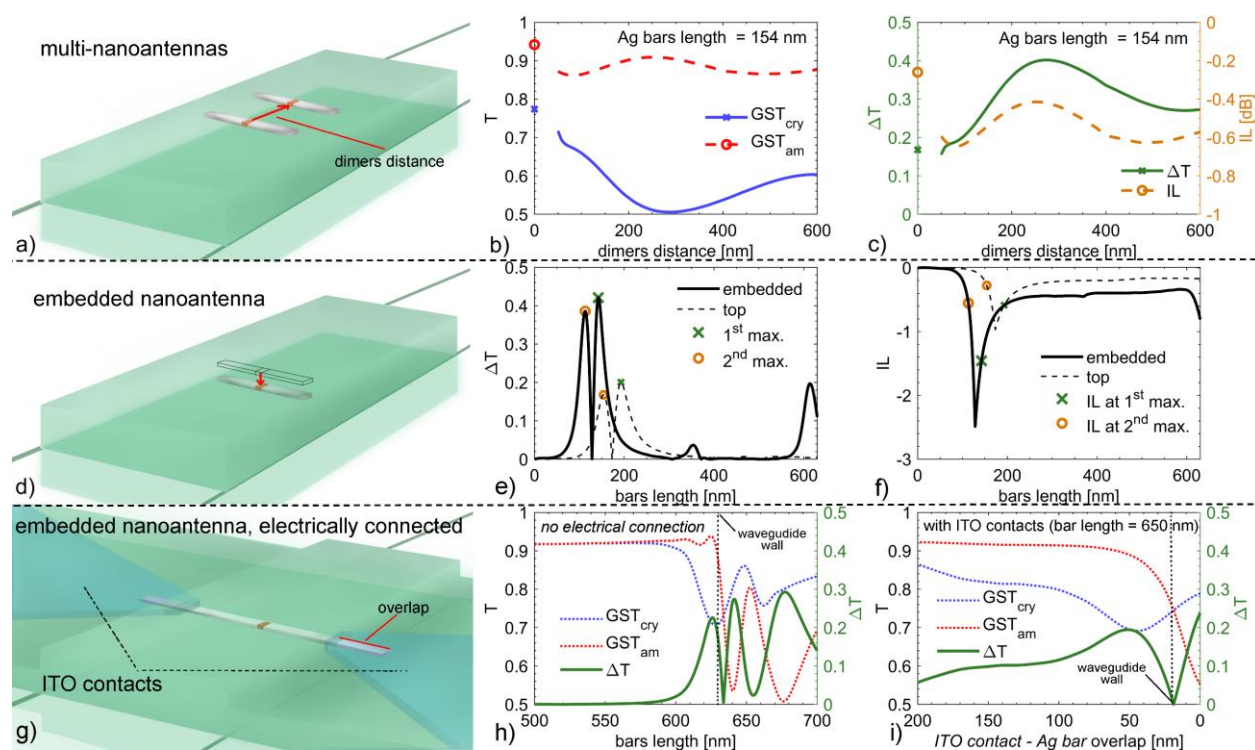

FIG. 6. Plasmonically-enhanced integrated photonic phase-change memory concepts increasing the theoretical optical contrast; the examples use a dimer-bars nanoantenna configuration, with gap width, bar width and thickness of 40 nm, 40 nm and 30 nm respectively. a) Pictorial representation of the double-dimer configuration. (b,c) Data obtained for the double-dimer solution using a fixed bars length of 154 nm, as a function of the centre-to-centre distance (as indicated in (a)). The degenerate solutions (at distance d = 0) represent the solution for a single nanostructure, reported as unique markers. b) Transmission data for the crystalline (blue) and amorphous (red, dashed) $Ge_2Sb_2Te_5$ PCM inclusion. c) Resulting optical contrast (left axis, green line; absolute units) and insertion loss (right axis, orange dashes line; dB units) theoretically obtainable after phase switching. d) Pictorial representation of the device embedded configuration. (e,f) Data obtained for the in-waveguide embedded solution. e) Optical contrast (absolute units) for the embedded configuration (continuous line), compared to the surface-bound device (dashed line). f) Correlated IL values for the embedded and top configurations. g) Pictorial representation of the mixed-mode operativity extension for the device in the embedded configuration, comprising two ITO contacts overlapping the Ag bars and interjecting the rib waveguide core. h) Transmission (left axis) and ΔT (right axis) data calculated in absence of the ITO contacts, for reference. i) Transmission (left axis) and ΔT (right axis) calculated for a fixed bar length of 650 nm, as a function of the ITO contact/Ag bar overlap (as indicated in (g)).

Finally, we turn our attention to technological issues linked with the fact that the highest performing, and most often used, plasmonic materials are gold and silver, both highly diffusive

12

metals. Indeed, gold is known to diffuse readily into both silicon and chalcogenides, alloying with both to form, for example, gold-silicides and gold-tellurides[59]. This in turn leads to deleterious effects in plasmonic PCM structures, suppressing optical resonances and leading to changes in PCM switching properties (crystallization temperatures). Diffusion, being a temperature-activated process, is worsened by the high-temperature dynamics involved during the PCM phase-switching process in which, for amorphization, the PCM must be heated to above its melting temperature.

To counteract the large diffusivity of high-performing plasmon-supporting metals, a few strategies can be pursued. One obvious approach is to place anti-diffusion barriers[51,59,60] between the plasmonic material and the PCM and/or any Si or diffusion-susceptible dielectric layers. Of course it is important that any such a diffusion barrier should not significantly alter, at least in a deleterious way, the optical or thermal properties of the device itself. Silicon nitride (Si_3N_4) has been shown to be a good barrier choice in this respect, since quite thin layers (< 10 nm) can provide sufficient diffusion protection[59].

A second obvious approach to the problem of the diffusion of plasmonic metals is to search for alternative, non-diffusive options. Any such options should ideally be CMOS-compatible, to allow for, ultimately, easy integration into PIC fabrication lines. Aluminium is one such material: it is a good plasmonic metal[61] and has already been used successfully for a number of CMOS-compatible plasmonic applications[62–64]. However, the melting temperature of Al, at 660^0C, is very close to that of most commonly used PCMs (e.g. $Ge_2Sb_2Te_5$ melts at 630^0C, $Ge_1Sb_2Te_4$ at 614^0C), thus there is a danger that during the PCM amorphization process any thermally adjacent Al plasmonic layer might also melt, leading to device degradation. To assess the suitability of other metals for integrated phase-change photonic device applications, we have therefore explored, in simulation, the optical performance (in terms of achievable (normalised) transmission contrast, ΔT, and insertion loss, IL) for a device consisting of a single dimer-bar antenna system (i.e. as shown in 6(d), and with the antenna on the top waveguide surface). The results are shown in FIG. 7, where, to limit the calculation range, only elemental materials are here considered.

As expected, the noble metals Au and Ag indeed show the best optical performance, with high optical contrast accompanied by a low IL. Aluminium also delivers good optical performance, as does copper; but Al has the previously mentioned problem of low melting point, and Cu is not very CMOS 'friendly'. FIG. 7 also highlights how nanoantenna materials with optical properties nearest those of a perfect-metal (i.e. low refractive index, high extinction coefficient) exhibit the best performances. Whilst none of the materials examined in FIG. 7 yield optical performances comparable to that of Au, Ag or Al, two CMOS compatible solutions with reasonable optical performances emerge, namely Tantalum and Niobium. Both these elements have attractively high melting temperatures, are relatively inert chemically and physically, and Nb has already been successfully demonstrated for plasmonic (free-space) perfect absorber applications[65]. Further

13

exploration of the potential suitability of Nb and Ta for integrated plasmonic phase-change photonic devices is thus recommended.
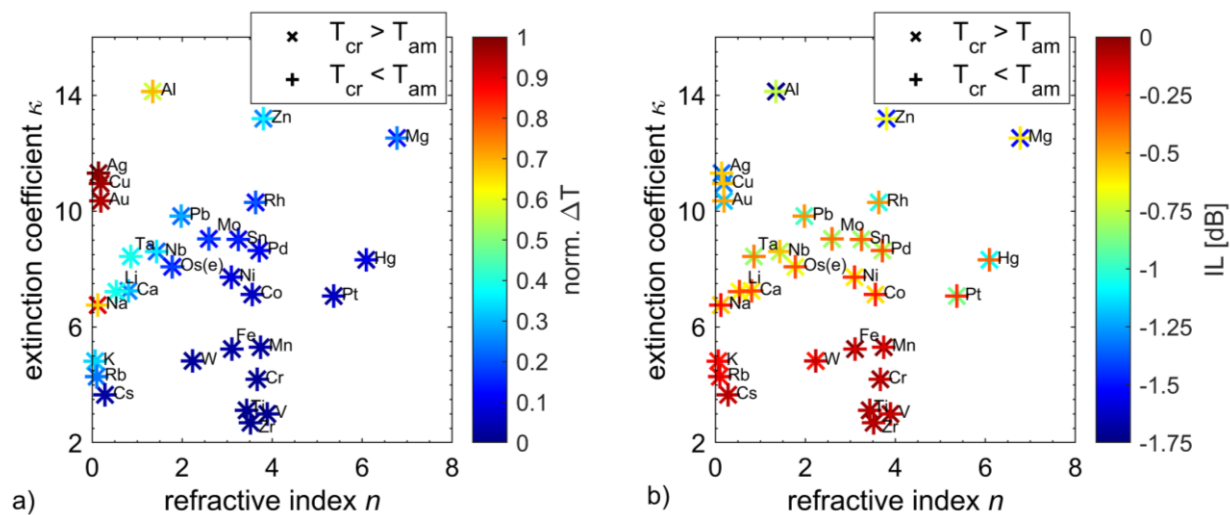

FIG. 7 Optical properties of the dimer (bars) plasmonically-enhanced integrated phase-change photonic memory device, as a function of the nanoantenna material. Two markers (vertical and diagonal crosses) are used, reporting the two values corresponding to the first and second |ΔT| peaks respectively. (a) Peak |ΔT| values (normalised to the maximum value obtained, here for Ag, of 45.9%). (b) IL calculated at the peak ΔT configuration.

V.   CONCLUSION

The co-integration of phase-change materials and plasmonics into the silicon photonics platform offers a promising route for the development of fast, low-power, integrated photonic memory and computing devices and systems. Silicon photonics enables low-latency, low-energy, high-bandwidth and parallelized on-chip signal transfer; plasmonic resonant structures can efficiently couple with the guided optical mode and squeeze the optical energy down to deep subwavelength features; and phase-change materials, thanks to their inherent non-volatile phase switching capabilities and the large change in optical properties (complex refractive index) that results from such switching, can tune the plasmonic resonant mode, in fact driving the nanoantenna optical response. In this short perspective paper, we underlined how the optimized combination of these various building blocks can lead to superior performances as compared to conventional, non-plasmonic, device designs. Indeed, improvements in terms of switching energy efficiency and speed in the range of one to two orders of magnitude were obtained. We also showed that the design-space for plasmonically-enhanced phase-change memory and computing devices is quite broad, with a wide range of appropriately configured nanoantenna structures (e.g. circular, bar and bow-tie type antennas; top-surface and embedded antenna types) yielding good optical

14

performance. Moreover, we showed how the electrical and optical domains can be brought together in so-called dual-mode, optical/electrical, device designs, where the PCM cell can be written and read in both domains. This could lead to easier integration of phase-change photonic devices and systems with our currently predominantly electronic computing world.

ACKNOWLEDGEMENT

DATA AVAILABILITY

Requests for data relating to the original results presented in the paper should be directed to the corresponding author.

REFERENCES

[1] M. Paniccia, M. Morse, and M. Salib, in *Silicon Photonics* (Springer Berlin Heidelberg, 2004), pp. 51–88.

[2] B. Jalali and S. Fathpour, J. Light. Technol. **24**, 4600 (2006).

[3] R. Soref, IEEE J. Sel. Top. Quantum Electron. **12**, 1678 (2006).

[4] R. Won, Nat. Photonics **4**, 498 (2010).

[5] D. Thomson, A. Zilkie, J.E. Bowers, T. Komljenovic, G.T. Reed, L. Vivien, D. Marris-Morini, E. Cassan, L. Virot, J.-M. Fédéli, J.-M. Hartmann, J.H. Schmid, D.-X. Xu, F. Boeuf, P. O'Brien, G.Z. Mashanovich, and M. Nedeljkovic, J. Opt. **18**, 073003 (2016).

[6] L. Chrostowski, H. Shoman, M. Hammood, H. Yun, J. Jhoja, E. Luan, S. Lin, A. Mistry, D. Witt, N.A.F. Jaeger, S. Shekhar, H. Jayatilleka, P. Jean, S.B. -d. Villers, J. Cauchon, W. Shi, C. Horvath, J.N. Westwood-Bachman, K. Setzer, M. Aktary, N.S. Patrick, R.J. Bojko, A. Khavasi, X. Wang, T. Ferreira de Lima, A.N. Tait, P.R. Prucnal, D.E. Hagan, D. Stevanovic, and A.P. Knights, IEEE J. Sel. Top. Quantum Electron. **25**, 1 (2019).

[7] C. Sun, M.T. Wade, Y. Lee, J.S. Orcutt, L. Alloatti, M.S. Georgas, A.S. Waterman, J.M. Shainline, R.R. Avizienis, S. Lin, B.R. Moss, R. Kumar, F. Pavanello, A.H. Atabaki, H.M. Cook, A.J. Ou, J.C. Leu, Y.H. Chen, K. Asanović, R.J. Ram, M.A. Popović, V.M. Stojanović, and others, Nature **528**, 534 (2015).

[8] C. Rios, P. Hosseini, C.D. Wright, H. Bhaskaran, and W.H.P. Pernice, Adv. Mater. **26**, 1372 (2014).

[9] C. Ríos, M. Stegmaier, P. Hosseini, D. Wang, T. Scherer, C.D. Wright, H. Bhaskaran, and

W.H.P.P. Pernice, Nat. Photonics **9**, 725 (2015).

[10] Z. Cheng, C. Ríos, W.H.P.P. Pernice, C.D. Wright, and H. Bhaskaran, Sci. Adv. **3**, e1700160 (2017).

[11] X. Li, N. Youngblood, C. Ríos, Z. Cheng, C.D. Wright, W.H. Pernice, and H. Bhaskaran, Optica **6**, 1 (2019).

[12] J. Feldmann, N. Youngblood, X. Li, C.D. Wright, H. Bhaskaran, and W.H.P. Pernice, IEEE J. Sel. Top. Quantum Electron. **26**, 1 (2019).

[13] C. Wu, H. Yu, H. Li, X. Zhang, I. Takeuchi, and M. Li, ACS Photonics **6**, 87 (2019).

[14] J. Feldmann, N. Youngblood, C.D. Wright, H. Bhaskaran, and W.H.P. Pernice, Nature **569**, 208 (2019).

[15] C. Ríos, N. Youngblood, Z. Cheng, M. Le Gallo, W.H.P. Pernice, C.D. Wright, A. Sebastian, and H. Bhaskaran, Sci. Adv. **5**, eaau5759 (2019).

[16] X. Li, N. Youngblood, Z. Cheng, S.G.-C. Carrillo, E. Gemo, W.H.P. Pernice, C.D. Wright, and H. Bhaskaran, Optica **7**, 218 (2020).

[17] J. Feldmann, N. Youngblood, M. Karpov, H. Gehring, X. Li, M. Le Gallo, X. Fu, A. Lukashchuk, A. Raja, J. Liu, and others, ArXiv Prepr. ArXiv2002.00281 (2020).

[18] J. Feldmann, M. Stegmaier, N. Gruhler, C. Ríos, H. Bhaskaran, C.D. Wright, and W.H.P.P. Pernice, Nat. Commun. **8**, 1256 (2017).

[19] I. Chakraborty, G. Saha, A. Sengupta, and K. Roy, Sci. Rep. **8**, 12980 (2018).

[20] I. Chakraborty, G. Saha, and K. Roy, Phys. Rev. Appl. **11**, 14063 (2019).

[21] N. Engheta, A. Salandrino, and A. Alù, Phys. Rev. Lett. **95**, 095504 (2005).

[22] P. Biagioni, J.-S. Huang, and B. Hecht, Reports Prog. Phys. **75**, 024402 (2012).

[23] A. Alù and N. Engheta, Nat. Photonics **2**, 307 (2008).

[24] Y. Gutiérrez, M. Losurdo, F. González, H.O. Everitt, and F. Moreno, J. Phys. Chem. C **124**, 7386 (2020).

[25] A.A. Maradudin, J.R. Sambles, and W.L. Barnes, *Modern Plasmonics* (Elsevier, 2014).

[26] S.A. Maier, Opt. Express **14**, 1957 (2006).

[27] S.M. Choudhury, D. Wang, K. Chaudhuri, C. DeVault, A. V. Kildishev, A. Boltasseva, and V.M. Shalaev, Nanophotonics **7**, 959 (2018).

[28] B. Dong, Y. Ma, Z. Ren, and C. Lee, J. Phys. D. Appl. Phys. **53**, 213001 (2020).

[29] F. Peyskens, A. Dhakal, P. Van Dorpe, N. Le Thomas, and R. Baets, ACS Photonics **3**, 102 (2016).

[30] D.A. Mohr, D. Yoo, C. Chen, M. Li, and S.-H. Oh, Opt. Express **26**, 23540 (2018).

[31] C. Chen, D.A. Mohr, H.K. Choi, D. Yoo, M. Li, and S.H. Oh, Nano Lett. **18**, 7601 (2018).

[32] M. Chamanzar, Z. Xia, S. Yegnanarayanan, and A. Adibi, Opt. Express **21**, 32086 (2013).

[33] Y. Luo, M. Chamanzar, A. Apuzzo, R. Salas-Montiel, K.N. Nguyen, S. Blaize, and A. Adibi, Nano Lett. **15**, 849 (2015).

[34] J. Kohoutek, A. Bonakdar, R. Gelfand, D. Dey, I. Hassani Nia, V. Fathipour, O.G. Memis, and H. Mohseni, Nano Lett. **12**, 2537 (2012).

[35] L. Elsinger, R. Gourgues, I.E. Zadeh, J. Maes, A. Guardiani, G. Bulgarini, S.F. Pereira, S.N. Dorenbos, V. Zwiller, Z. Hens, and D. Van Thourhout, Nano Lett. **19**, 5452 (2019).

[36] B. Wang, S. Blaize, and R. Salas-Montiel, Nanoscale **11**, 20685 (2019).

[37] Z. Li, M.-H.H. Kim, C. Wang, Z. Han, S. Shrestha, A.C. Overvig, M. Lu, A. Stein, A.M. Agarwal, M. Lončar, and N. Yu, Nat. Nanotechnol. **12**, 675 (2017).

[38] C. Yao, S.C. Singh, M. ElKabbash, J. Zhang, H. Lu, and C. Guo, Opt. Lett. **44**, 1654 (2019).

[39] D. Vercruysse, P. Neutens, L. Lagae, N. Verellen, and P. Van Dorpe, ACS Photonics **4**, 1398 (2017).

[40] A. Espinosa-Soria, E. Pinilla-Cienfuegos, F.J. Díaz-Fernández, A. Griol, J. Martí, and A. Martínez, ACS Photonics **5**, 2712 (2018).

[41] M. Castro-Lopez, N. de Sousa, A. Garcia-Martin, F.Y. Gardes, and R. Sapienza, Opt. Express **23**, 28108 (2015).

[42] J.E. Muench, A. Ruocco, M.A. Giambra, V. Miseikis, D. Zhang, J. Wang, H.F.Y. Watson, G.C. Park, S. Akhavan, V. Sorianello, M. Midrio, A. Tomadin, C. Coletti, M. Romagnoli, A.C. Ferrari, and I. Goykhman, Nano Lett. **19**, 7632 (2019).

[43] C. Haffner, W. Heni, Y. Fedoryshyn, J. Niegemann, A. Melikyan, D.L. Elder, B. Baeuerle, Y. Salamin, A. Josten, U. Koch, C. Hoessbacher, F. Ducry, L. Juchli, A. Emboras, D. Hillerkuss, M. Kohl, L.R. Dalton, C. Hafner, and J. Leuthold, Nat. Photonics **9**, 525 (2015).

[44] M. Burla, C. Hoessbacher, W. Heni, C. Haffner, Y. Fedoryshyn, D. Werner, T. Watanabe, H. Massler, D.L. Elder, L.R. Dalton, and J. Leuthold, APL Photonics **4**, 056106 (2019).

[45] R. Amin, R. Maiti, Y. Gui, M. Miscuglio, E. Heidari, R.T. Chen, H. Dalir, and V.J. Sorger, in *Conf. Lasers Electro-Optics* (OSA, Washington, D.C., 2020), p. FM2R.2.

[46] U. Koch, C. Uhl, H. Hettrich, Y. Fedoryshyn, C. Hoessbacher, W. Heni, B. Baeuerle, B.I. Bitachon, A. Josten, M. Ayata, H. Xu, D.L. Elder, L.R. Dalton, E. Mentovich, P. Bakopoulos, S. Lischke, A. Krüger, L. Zimmermann, D. Tsiokos, N. Pleros, M. Möller, and J. Leuthold, Nat. Electron. **3**, 338 (2020).

[47] M. Thomaschewski, Y. Yang, C. Wolff, A.S. Roberts, and S.I. Bozhevolnyi, Nano Lett. **19**, 1166 (2019).

[48] A. V. Krasavin and N.I. Zheludev, Appl. Phys. Lett. **84**, 1416 (2004).

[49] M. Rudé, R.E. Simpson, R. Quidant, V. Pruneri, and J. Renger, ACS Photonics **2**, 669 (2015).

[50] A. Emboras, J. Niegemann, P. Ma, C. Haffner, A. Pedersen, M. Luisier, C. Hafner, T. Schimmel,

17

and J. Leuthold, Nano Lett. **16**, 709 (2016).

[51] C. Ruiz de Galarreta, S.G.-C. Carrillo, Y.-Y. Au, E. Gemo, L. Trimby, J. Shields, E. Humphreys, J. Faneca, L. Cai, A. Baldycheva, J. Bertolotti, and C.D. Wright, J. Opt. **22**, 114001 (2020).

[52] Z. Zhang, J. Yang, W. Bai, Y. Han, X. He, J. Zhang, J. Huang, D. Chen, S. Xu, and W. Xie, J. Nanophotonics **13**, 1 (2019).

[53] M. Singh, S.K. Raghuwanshi, and T. Srinivas, Phys. Lett. A **383**, 3196 (2019).

[54] E. Gemo, S.G.-C. Carrillo, C.R. De Galarreta, A. Baldycheva, H. Hayat, N. Youngblood, H. Bhaskaran, W.H.P. Pernice, and C.D. Wright, Opt. Express **27**, 24724 (2019).

[55] E. Gemo, S. García-Cuevas Carrillo, J. Faneca, C. Ruíz de Galarreta, H. Hayat, N. Youngblood, A. Baldycheva, W.H.P. Pernice, H. Bhaskaran, and C.D. Wright, in *Photonic Phononic Prop. Eng. Nanostructures X*, edited by A. Adibi, S.-Y. Lin, and A. Scherer (SPIE, 2020), p. 50.

[56] N. Farmakidis, N. Youngblood, X. Li, J. Tan, J.L. Swett, Z. Cheng, C.D. Wright, W.H.P. Pernice, and H. Bhaskaran, Sci. Adv. **5**, eaaw2687 (2019).

[57] E. Yalon, S. Deshmukh, M. Muñoz Rojo, F. Lian, C.M. Neumann, F. Xiong, and E. Pop, Sci. Rep. **7**, 1 (2017).

[58] Y.-H. Jin, B.J. Park, and M.-K. Kim, Opt. Express **24**, 25540 (2016).

[59] L. Lu, W. Dong, J.K. Behera, L. Chew, and R.E. Simpson, J. Mater. Sci. **54**, 2814 (2019).

[60] B. Gholipour, J. Zhang, K.F. MacDonald, D.W. Hewak, and N.I. Zheludev, Adv. Mater. **25**, 3050 (2013).

[61] M.W. Knight, N.S. King, L. Liu, H.O. Everitt, P. Nordlander, and N.J. Halas, ACS Nano **8**, 834 (2014).

[62] B.Y. Zheng, Y. Wang, P. Nordlander, and N.J. Halas, Adv. Mater. **26**, 6318 (2014).

[63] A. Manolis, P.J. Cegielski, L. Markey, J.-C. Weeber, A. Dereux, N. Pleros, E. Chatzianagnostou, G. Dabos, D. Ketzaki, D. Tsiokos, B. Chmielak, S. Suckow, A.L. Giesecke, and C. Porschatis, J. Light. Technol. **37**, 5516 (2019).

[64] C.R. de Galarreta, A.M. Alexeev, Y.-Y. Au, M. Lopez-Garcia, M. Klemm, M. Cryan, J. Bertolotti, and C.D. Wright, Adv. Funct. Mater. **28**, 1704993 (2018).

[65] S. Bagheri, N. Strohfeldt, M. Ubl, A. Berrier, M. Merker, G. Richter, M. Siegel, and H. Giessen, ACS Photonics **5**, 3298 (2018).

18